JCTC Journal of Chemical Theory and Computation

Order−Disorder Transition and Phase Separation in the MgB_2 Metallic Sublattice Induced by Al Doping

S. Brutti* and G. Gigli

Dipartimento di Chimica, Dipartimento di Chimica, Sapienza Università di Roma, P.le Aldo Moro 5 00185 Roma, Italy

Received January 20, 2009

Abstract: MgB_2 is a superconductor constituted by alternating Mg and B planar layers: doping of both the sublattices has been observed experimentally to destroy the outstanding superconductive properties of this simple material. In this study we present the investigation by first principles methods at atomistic scale of the phase separation induced by aluminum doping in the MgB_2 lattice. The calculations were performed by Density Functional Theory in generalized gradient approximation and pseudopotentials. Orthorhombic oP36 supercells derived by the primitive hR3 MgB_2 cell were built in order to simulate the aluminum−magnesium substitution in the 0−50% composition range. The computational results explained the occurrence of a phase separation in the $Mg_{1-x}Al_xB_2$ system. The miscibility gap is predicted to be induced by an order−disorder transition in the metallic sublattice at high Al concentration. Indeed at 1000 K aluminum substitution takes place on random Mg sites for concentration up to 17% of the total metallic sites, whereas at Al content larger than 31% the substitution is energetically more favorable on alternated metallic layers (Mg undoped planes alternate with Mg−Al layers). The formation of this Al-rich phase lead at 50% doping to the formation of the double omega $Mg_{1/2}Al_{1/2}B_2$ ordered lattice. From 17 to 31% the two phases, the disordered $Mg_{1-x}Al_xB_2$ ($x < 0.17$) and the ordered $Mg_{1/2+y}Al_{1/2-y}B_2$ ($y < 0.19$) lattices, coexist. This phase separation is driven by the balance of the enthalpy and entropy contributions to the Gibbs energy. Present DFT-GGA calculations indicate that this thermodynamically predicted suppression of the Al doping disorder in the metallic sublattice of MgB_2 occurs in parallel with the collapse of the superconductive properties of the material.

Introduction

Magnesium diboride, MgB_2, was observed to undergo a superconductive transition at $T_c = 39$ K, one of the highest known transition temperatures for a noncopper-oxide material.[1] This finding boosted the interest in this simple compound, and stimulated research efforts mainly focused on the physical and thermodynamic properties (i.e., energetic stability, thermal conductivity, elastic and electric properties, electronic and crystal structure, e.g. refs 2 and 3) as well as fabrication, in particular, film growth processing (e.g., ref 4).

The electronic structure of MgB_2 is now well understood: the Fermi surface consists of two three-dimensional sheets due to the π bonding and antibonding bands and two nearly cylindrical sheets due to the two-dimensional σ bands. Its superconductivity properties arise from a phonon mediated mechanism, with different coupling strengths, with the two mentioned σ and π electronic bands, which leads to the uncommon appearance of two distinct superconducting gaps.[5,6] In the past few years the substitution of Mg with Al, Ca, Li and Sc, and B with C has been investigated to understand the evolution of the pairing process (e.g., refs 7−10). The various attempts to obtain compounds with higher T_c derived by doping from MgB_2 have been up to the present unsuccessful, suggesting that MgB_2 may represent a unique combination of events where electronic and dynamic properties reach an extremely favorable balance.[11] Moreover

* Corresponding author e-mail: sergio.brutti@uniroma1.it.

10.1021/ct900167k CCC: $40.75
Published on Web 06/05/2009

MgB_2, due to its very simple crystal and electronic structure, is even a fortunate example of a two-gap superconductor where the effect of doping on the electronic structure can be accurately calculated by first principles methods: this makes the MgB_2 system a typical case study.[12]

There is experimental evidence[13−16] of a phase separation in the $Mg_{1-x}Al_xB_2$ system in the x=0.1−0.4 range. This separation is apparently related to the precipitation of a ternary Al-rich phase with a superstructure related to the MgB_2 lattice with doubled c-axis, similar to the crystalline double-ω phase $Mg_{0.5}Al_{0.5}B_2$.[17] The crystal chemistry and its correlation with the functional properties of the substituted MgB_2 phase by aluminum and other doping atoms has been the object of a number of computational investigations.[18−23] Nevertheless a detailed interpretation at the atomistic level of both the lattice distortion related to the phase separation and the driving forces that lead to the establishing of this multiphase equilibrium are still missing. This is the object of this paper where we present the results of the investigation by first principles methods of the lattice stability of the $Mg_{1-x}Al_xB_2$ (0<x<0.5) system. The electronic structure calculations have been carried out by means of Density Functional Theory (DFT), using supercells. The goal is the analysis of the phase separation due to the modulation of the composition of MgB_2 by Al doping. This will be characterized by considering the lattice configurations at different doping concentrations in order to give a structural interpretation at the atomistic level. The driving force that, from a thermodynamic point of view, promotes the phase separation will be analyzed in terms of free energy by distinguishing enthalpy and entropy contributions.

Computational Method

The study of the lattice stability of the $Mg_{1-x}Al_xB_2$ (0<x<0.5) system has been carried out by spin unpolarized electronic structure calculations within the density functional theory (DFT) approach, in the generalized-gradient approximation (GGA-PW91),[24] and using pseudopotentials for core electrons.

MgB_2 has an hP3 primitive cell (C32 strukturbericht designation) with space group *P6/mmm* (no. 191) and Mg and B atoms in the 1a (0 0 0) and 2d ($^1/_3,^2/_3,^1/_2,^2/_3,^1/_3,^1/_2$) sites, respectively. The corresponding standard hexagonal axes ($\hat{A}_1,\hat{A}_2,\hat{A}_3$) in terms of Cartesian versors ($\hat{x},\hat{y},\hat{z}$) are

$$\hat{A}_1 = {}^1/_2 a\hat{x} - {}^{\sqrt{3}}/_2 a\hat{y}$$

$$\hat{A}_2 = {}^1/_2 a\hat{x} - {}^{\sqrt{3}}/_2 a\hat{y}$$

$$\hat{A}_3 = c\hat{z}$$

The study of the aluminum doping has been carried out by using the supercells approach: in particular a oP36 supercell has been derived from the primitive hP3 MgB_2 lattice by the following transformation

$$\hat{A}_1^* = \hat{A}_1 - \hat{A}_2$$

$$\hat{A}_2^* = -3 \cdot (\hat{A}_1 - \hat{A}_2)$$

$$\hat{A}_2^* = -2 \cdot \hat{A}_3$$

where ($\hat{A}_1^*,\hat{A}_2^*,\hat{A}_3^*$) are the novel axes derived from the primitive vectors ($\hat{A}_1,\hat{A}_2,\hat{A}_3$). The resultant supercell axes in terms of Cartesian versors and primitive cell parameters are

$$\hat{A}_1^* = \sqrt{3} \cdot a\hat{x}$$

$$\hat{A}_2^* = -3 \cdot a\hat{y}$$

$$\hat{A}_3^* = -2 \cdot c\hat{z}$$

Both the primitive cell and the supercell are presented in Figure 1a and b.

In summary the orthorhombic supercell results from the merge of 12 primitive hexagonal cells: the new periodic unit consists of an alternated couple of metallic and boron layers. The oP36 structure has 12 metallic sites (Figure 1c). By following the designation outlined in Figure 1c for the metallic sites in the oP36 lattice, the corresponding site coordinates are as follows: (1) 0 0 0; (2) 1/2; 1/6 0; (3) 0 1/3 0; (4) 1/2; 1/2 0; (5) 0 2/3 0; (6) 1/2 5/6 0; (a) 0 0 1/2; (b)1/2 1/6 1/2; (c) 0 1/3 1/2; (d) 1/2, 1/2, 1/2; (e) 0 2/3 1/2; (f) 1/2, 5/6, 1/2. As a consequence 7 different compositions in the $Mg_{1-x}Al_xB_2$ (0<x<0.5) ternary system can be simulated (i.e., 0, 1/12, 2/12, 3/12, 4/12, 5/12, 6/12) as well as the lattice of the double omega $Mg_{0.5}Al_{0.5}B_2$ phase (Figure 1d). The seven intermediate compositions are obviously obtained by substituting the necessary number of Mg atoms by Al. It is to be noted that the number of configurations that represents the occurring substitutions, increases as the concentration of the doping Al increases. In the oP36 supercell, the p aluminum and $(n-p)$ magnesium atoms are accommodated in $n = 12$ metallic sites: the resulting number of configurations is $\zeta = (n!)/(p!(n-p)!)$. From a crystallographic point of view each configuration represents an unique chemical prototype. As a consequence at a given doping concentration

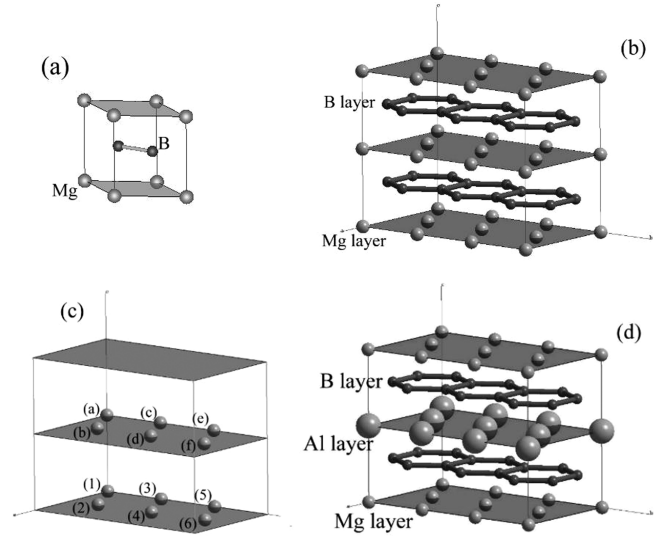

Figure 1. (a) MgB_2 primitive cell hP3; (b) $(MgB_2)_{12}$ supercell oP36; (c) 12 Mg sites in the oP36 supercell; (d) $(Mg_{0.5}Al_{0.5}B_2)_{12}$ double omega-based structure supercell oP36.

Table 1. Irreducible Supercells Simulated by DFT Calculations

x Al content in the $Mg_{1-x}Al_xB_2$ system	number of Al doping atoms	oP36 supercell designation	doping character	Al substituted metallic sites
0.0	0	oP36(0)[a]	-	-
0.083	1	oP36(1)	-	(1)
0.166	2	oP36(2V)oP36(2L)	in-volume in-layer	(1)-(d) (1)-(4)
0.25	3	oP36(3V)oP36(3L)	in-volume in-layer	(1)-(d)-(4) (1)-(4)-(2)
0.333	4	oP36(4V)oP36(4L)	in-volume in-layer	(1)-(d)-(4)-(a) (1)-(4)-(2)-(6)
0.416	5	oP36(5V)oP36(5L)	in-volume in-layer	(1)-(d)-(4)-(a)-(3) (1)-(4)-(2)-(6)-(3)
0.50	6	oP36(6V)oP36(6L)[b]	in-volume in-layer	(1)-(d)-(4)-(a)-(3)-(f)(1)-(4)-(2)-(6)-(3)-(5)
1.0	12	oP36(12)[c]	-	all

[a] This configuration corresponds to the hP3 MgB_2 phase. [b] This configuration corresponds to the double omega $Mg_{0.5}Al_{0.5}B_2$ phase. [c] This configuration corresponds to the hP3 AlB_2 phase.

the number of inequivalent supercells to be simulated becomes rather large, the configurations being 1, 12, 66, 220, 495, 792, 924, for 0, 1, 2, 3, 4, 5, 6 Al substitutions, respectively. Symmetry considerations can lead to a reduction of the supercells to be considered: as an example, in the case of our oP36 supercell, the symmetry-irreducible structural permutations, for 0, 1, 2, 3, 4 substitutions, are 1, 1, 7, 13 and 36, respectively. However, although the resulting number of inequivalent configurations is reduced, they are still too many to allow a complete and easy screening of all the configurations.

On considering these constraints, in order to draw a reliable picture at the atomistic scale of the $Mg_{1-x}Al_xB_2$ ($0<x<0.5$) ternary system, two symmetry-inequivalent configurations were considered for each composition. This choice aimed at taking into account the alternative and concurrent in-layer and in-volume doping. Indeed for a multiple aluminum substitution, the doping can occur on a single metallic layer (in-layer doping), leaving the other Mg layer in the oP36 structure unaltered, or on both metallic planes (in-volume doping). Among all the possible in-volume or in-layer substituted structures, we apply another "selection rule", by adopting the configuration in which the interatomic Al−Al distance is maximized. This rather arbitrary assumption aims to mimic a "minimum-perturbation criteria" of the hosting MgB_2 lattice, by minimizing the direct interaction between the aluminum atoms and the resulting chemical pressure. The thirteen supercells selected with these criteria for the DFT calculations are summarized in Table 1.

DFT calculations have been performed by using the PWscf code, included in the QUANTUM-ESPRESSO package:[25] post-SCF calculations were carried out by using the routines included in the same package. Vanderbilt ultrasoft pseudopotentials were adopted for Mg, Al, and B including 8, 3, and 3 electrons in the valence shells, respectively. The adopted pseudopotentials were retrieved from the database provided by the PWscf compilers.[25]

The Irreducible Brillouin Zone (IBZ) was sampled by adopting Γ-centered uniform Monkhorst-Pack (MP) k-points grids.[26] A $7 \times 7 \times 7$ grid with 64 irreducible k-points has been adopted for the oP36 supercells. The tetrahedron method[27] has been adopted for deriving the electron occupancies in the IBZ integration at the Fermi level.

The adopted pseudopotentials were checked on the boron, magnesium, and aluminum isolated atoms and elemental bulks in order to assess a satisfactory kinetic energy cutoff, E_{cut}, for the plane wave basis set calculations: a total energy convergence threshold of 0.3 mRy at^{-1} was achieved using energy cutoffs of 29 and 116 Ry for the electron wave functions and charge density, respectively. The adopted total energy convergence threshold in the self-consistent field calculations was 10^{-8} Ry. All the elemental Al(fcc), Mg(hcp),[28] and β-B[29] lattices were fully relaxed, optimizing the cell parameters and the atomic positions: the relevant convergence threshold on the pressure was set at 0.2 kbar. The MP grid meshes, and irreducible k-points adopted for elemental bulk calculations were $15 \times 15 \times 15$ (120), $17 \times 17 \times 17$ (297), and $5 \times 5 \times 5$ (63) for Al, Mg, and B, respectively. It is to be noted that for the β-B structure the triclinic lattice proposed in ref 29 derived from the classical trigonal structure was adopted.

The computed cell parameters are in agreement with the experimental literature values within 0.5% and the cohesion energies within 2.5% in the case of Al and Mg, whereas triclinic boron cohesion energy is overestimated by about 40 kJ mol at^{-1}, approximately 7% of the experimental value.[30] However it is to be noted that recently van Setten and co-workers[29] reported a detailed study about the stability of elemental boron polymorphic structures and in particular the β-B lattice. These authors observed that more than 16 boron allotropes exist and that, from a theoretical point of view, a complete picture of the lattice stabilities of this simple system is still far from being assessed due to the complex structure of the β-boron primitive lattice.

As a consequence we performed a further check of the reliability of the computational condition adopted by simulating the MgB_2 hP3 primitive lattice (MP grid $15 \times 15 \times 15$ with 216 irreducible k-points). The optimized cell parameters *a* and *c* are 3.0750 ± 0.0001 Å and 3.5360 ± 0.0002 Å to be compared to the experimental values of 3.083 ± 0.001 Å and 3.520 ± 0.001 Å:[28] the disagreement is in both cases smaller than 0.5%. For what concerns the enthalpy of formation the benchmark is the experimental value -41.5 ± 0.5 kJ mol at^{-1}.[3] It is to be noted that two different energy reference states can be adopted in order to derive the enthalpy of formation of the MgB_2 phase: (i) the sum of the isolated atoms total energies or (ii) the sum of the elemental bulk total energies. In the first case the auxiliaries thermodynamic properties (i.e., the enthalpy of formation of the isolated atoms) can be retrieved from a standard thermodynamic database.[30] The computed formation enthalpy for the hP3 MgB_2 phase are -42.5 ± 2.0 and -18.5 ± 0.1 kJ mol at^{-1},

Table 2. Computational Results: Structural Parameters and Energetics

	in-volume Al doped supercells				in-plane Al doped supercells			
x Al in the $Mg_{1-x}Al_xB_2$ system		*a*[Å]	*c*[Å]	$\Delta_fH°_{0K}$[kJ mol at^{-1}]		*a*[Å]	*c*[Å]	$\Delta_fH°_{0K}$[kJ mol at^{-1}]
0.0	oP36(0)	3.076[a]	3.537[a]	−42.3[a]				
0.083	oP36(1)	3.072	3.498	−42.6				
0.166	oP36(2 V)	3.067	3.460	−42.8	oP36(2 L)	3.067	3.462	−43.0
0.25	oP36(3 V)	3.064	3.420	−42.9	oP36(3 L)	3.062	3.432	−43.6
0.333	oP36(4 V)	3.060	3.384	−43.1	oP36(4 L)	3.054	3.409	−44.4
0.416	oP36(5 V)	3.053	3.361	−43.3	oP36(5 L)	3.046	3.388	−45.1
0.50	oP36(6 V)	3.044	3.343	−43.2	oP36(6 L)	3.037[b]	3.372[b]	−45.6[b]
1.0	oP36(12)	3.001[c]	3.282[c]	−37.1[c]				

[a] Undoped MgB_2 structure [oP36(0)]; experimental values[28] $a = 3.083$ Å; $c = 3.521$ Å. [b] Double-ω $Mg_{0.5}Al_{0.5}B_2$ structure; experimental values[28] $a = 3.044$ Å; $c = 3.356$ Å. [c] Fully doped AlB_2 structure[oP36(12)]; experimental values[28] $a = 3.005$ Å; $c = 3.257$ Å.

for the (i) and (ii) reference state, respectively. As expected the unsatisfactory prediction of the β-B cohesion energy directly propagates to the heat of formation of the hP3 phase resulting in a large underestimation of the experimental value. On the other hand by adopting the isolated atoms as a reference state the experimental formation enthalpy and the DFT data are in excellent agreement within 1.0 kJ mol at^{-1}. As a consequence for the supercell calculations we preferred to adopt as energy reference state the isolated atoms rather than the elemental bulk lattices.

Similarly to the cases of the bulk elements the supercells were fully relaxed, optimizing both the atomic positions and the cell parameters. In the optimization of the atomic positions, the total energy convergence threshold was set at 10^{-5} Ry, and the convergence threshold on forces acting on the atoms was set at 10^{-4} Ry. The cell parameters were relaxed with respect to a convergence threshold on the pressure set at 0.2 kbar, to be satisfied by each component of the 3×3 stress matrix.

Using these computational conditions the total energy for all the oP36 supercells was converged to better than 0.3 mRy at^{-1} in comparison with data obtained with a $5 \times 5 \times 5$ MP grid and $E_{cut} = 28$ Ry.

Calculations Results

The computational results are summarized in Table 2. The cell parameters are those of the corresponding reduced primitive hP3 lattice: these have been obtained by using the inverse crystal transformation discussed in the previous section. The energy stabilities are presented as heat of formation at 0 K. The comparison with previous experimental data from the literature is satisfactory both for what concerns the structural trends of the *a* and *c* cell parameters in the entire composition range (see refs 14 and 15) and for the energetic stabilities of the MgB_2, $Mg_{0.5}Al_{0.5}B_2$, and AlB_2 phases (see refs 3, 12, and 31). The lattice parameters matched in all cases the experimental values within 0.5%.

From a structural point of view the differences between in-plane and in-volume doped supercells appears minor in the case of the *a*-axis trends, whereas the *c*-axis comparison evidences a more compact structure for the in-volume doping case. These prediction are somewhat expected since the *a*-axis modifications are limited by the rigid covalent B−B honeycomb network, whereas the *c*-axis variations are related to changes in the stacking among the alternated metallic-boron planar layers. Indeed DFT calculations correctly predict that the metal−boron layer distances along the *c*-axis are expanded in the case of MgB_2 (oP36(0)) and compressed for the AlB_2 lattice (oP36(12)). In the intermediate cases the in-volume doping allows the relaxation of all the interlayer distances, whereas the in-plane substitution keeps unaltered one Mg-layer resulting in an uncompressed B−Mg−B stacking only partially compensated by the relaxation of the adjacent B-(Mg,Al)-B stacking planes.

From a thermodynamic point of view the comparison between the formation energy of the in-volume and in-plane doped supercells reported in Figure 2a makes clear that these last lattices are in all cases energetically more stable, suggesting that the Al atoms in the MgB_2 lattice cluster preferentially on single metallic layers leaving unaltered alternated Mg-planes. However in order to draw a conclusion about the thermodynamic equilibria between the in-plane/in-volume substituted phases, the entropy contribution must be taken into account, and therefore some further discussion concerning the configuration entropy is needed.

As discussed in the previous section the substitution of the magnesium atoms by aluminum in the oP6 lattice can occur in 12 metallic sites leading to a number of structural configurations increasing with the doping concentration. Similarly to the case of random or ordered alloys, the resulting entropy contribution deserves to be accounted for predicting the thermodynamic stability of the various lattices that is driven at a given temperature by the Gibbs energy. Therefore, by neglecting the vibrational contributions at finite temperature for the oP36 lattices formation enthalpy and entropy, both partially compensated by the elemental bulk atoms concurrent effects, the Gibbs energy of formation for a generic *i* supercell can be approximated by $\Delta_f G^o_{T,i} = \Delta_f H^o_{0K,i}(DFT) - T \cdot S_{conf,i}$, where $S_{conf,i}$ is the corresponding *i*-th configurational entropy.

The configurational entropy is $S_{conf} = R \cdot \ln \zeta$, where ζ are the structural permutations of the Al and Mg atoms in the N metallic sites in the oP36 lattice at a given doping concentration. Under periodic conditions at the continuum limit the configurational entropies for the in-volume and in-plane doped structures are given at any concentration by

$$S_{conf}^{involume} = -\frac{R}{3} \cdot [(1 - \chi_{Al}) \cdot \ln(1 - \chi_{Al}) + \chi_{Al} \cdot \ln \chi_{Al}]$$

$$S_{conf}^{inplane} = -\frac{R}{6} \cdot [(1 - 2 \cdot \chi_{Al}) \cdot \ln(1 - 2 \cdot \chi_{Al}) + 2 \cdot \chi_{Al} \cdot \ln(2 \cdot \chi_{Al})]$$

where R is the gas constant, and χ_{Al} is the molar fraction of aluminum in the system. The $^1/_3$ and $^1/_6$ factors normalize the configurational entropies per mole of atoms. The plots of the configurational entropies in the two cases are presented in Figure 2b as a function of the doping concentration.

The formation enthalpies at intermediate concentrations were obtained by a linear interpolation of the in-volume and in-plane DFT values reported in Table 2 for the 0.083, 0.166, 0.25, 0.333, 0.416, 0.5 Al content in the $Mg_{1-x}Al_xB_2$ system.

An example of the resulting Gibbs energy plot at 1000 K is presented in Figure 2c. The crossing between the two Gibbs energy curves at 1000 K for the in-plane and in-volume doped structures indicates the presence of two single phase stability regions. Indeed starting from the MgB_2 pure lattice for Al contents <17% the Gibbs energy of the in-volume doped structures is larger than the corresponding one for the in-plane substituted lattices. In this region the doping is predicted to occur randomly driven by the larger configuration entropy of the in-volume doping compared to the in plane substitution. A reverse picture is observed for Al concentration >31% where the Gibbs energy curve of the in-plane doped lattices is more negative than the corresponding one for the in-volume doping. In this region DFT calculations predicts the clustering of the Al atoms on single planes alternated with unaltered Mg-layers: this ordering transition is driven by the larger formation enthalpy of the in-plane doping compared to the in volume doped lattices. In the intermediate compositions 17−31 Al at.% the Gibbs energy plot predicts the occurring of a phase separation stability field. Indeed in this doping range it is possible to draw a common tangent line to the two Gibbs energy curves. This tangent line represents the total Gibbs energy of a system constituted by a mechanical mixture of the two in-volume and in-plane lattices, both at fixed Al concentration: 17 and 31 at.% Al, respectively. In the 17−31% composition range the mixture is predicted to be the thermodynamically stable system being its Gibbs energy smaller than those of the in-volume or in-plane doped lattices at the same overall Al doping concentration. A similar analysis can be repeated at any temperature: the resulting phase diagram is shown in Figure 3a.

In summary, going from pure MgB_2 to $Mg_{0.5}Al_{0.5}B_2$, our calculations predict that at small Al concentrations the C32

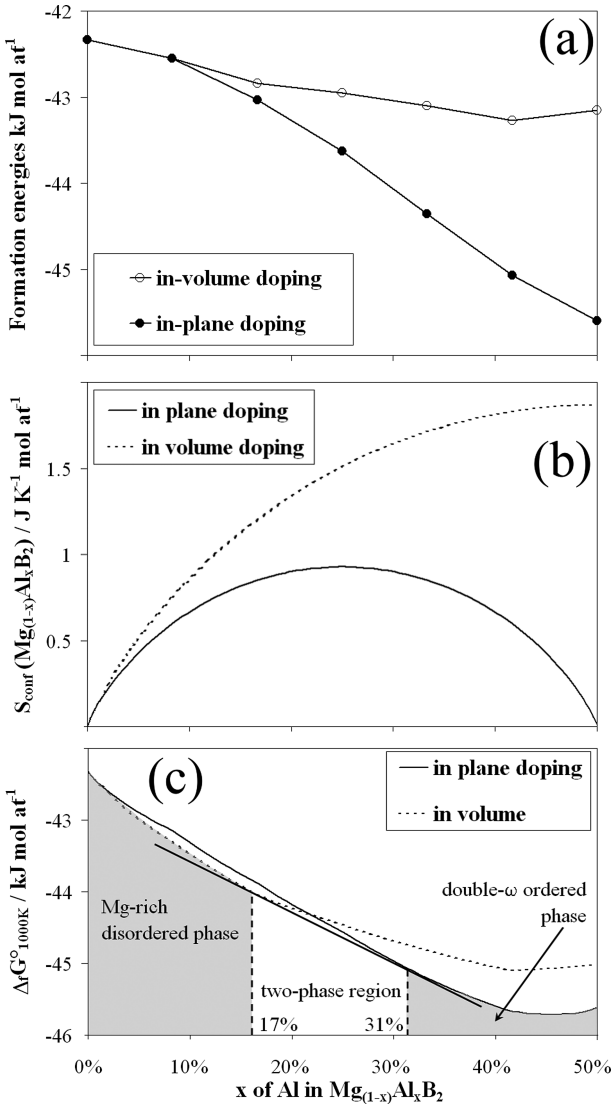

Figure 2. (a) DFT formation energies for the in-plane and in-volume aluminum doped supercells. (b) Configurational entropy for the in-plane or in-volume doping of the MgB_2 phase in the 0−50 Al at% composition range. (c) Predicted Gibbs energy plot and phase diagram at 1000 K for the $Mg_{1-x}Al_xB_2$ system.

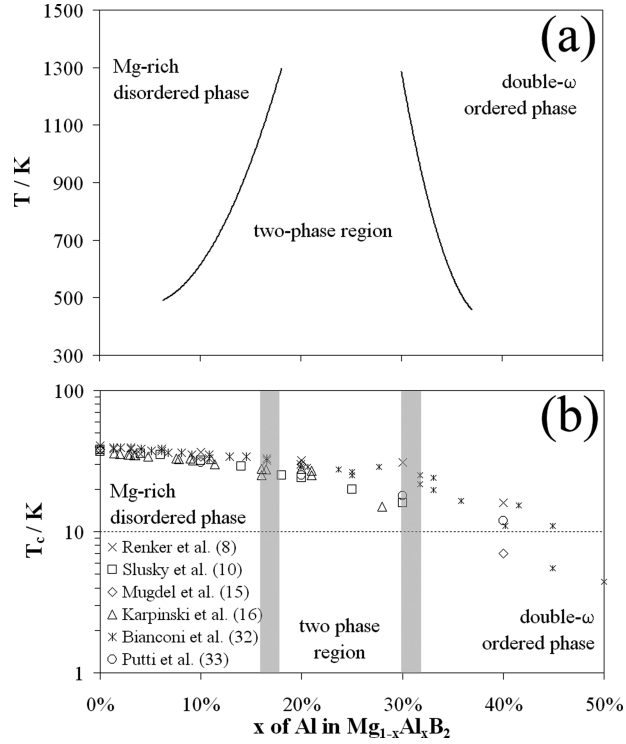

Figure 3. (a) Predicted phase diagram for the $Mg_{1-x}Al_xB_2$ system in the 0−50 at.% Al composition range. (b) Experimental literature superconductive T_c for the $Mg_{1-x}Al_xB_2$ system. The two gray areas represent the predicted intervals of the two-phase region boundaries in the high temperatures range 1000−1300 K. This temperature range is typically used in the synthesis of the $Mg_{1-x}Al_xB_2$ samples.

lattice, driven by configurational entropy, would host randomly the doping atoms resulting in a disordered metallic sublattice. At large Al content the ordering of the doping atoms in a double-ω-like structure is energetically more favored. At intermediate concentration the two disordered and ordered structures coexist: the phase borders are temperature dependent and range between 4−18% and 37−30% for the disordered/two-phase and the two-phase/ordered boundaries, respectively, in the temperature range 450−1300 K.

Discussion and Conclusions

In this paper we presented the analysis of the lattice stability of the $Mg_{1-x}Al_xB_2$ system by DFT and supercells approach. The computational results predict, in agreement with the experimental literature, the occurrence of a phase separation in the $Mg_{1-x}Al_xB_2$ system. The miscibility gap is predicted to be induced by a disorder−order transition in the metallic sublattice at high Al concentration. Indeed at 1000 K aluminum substitution takes place on random Mg sites for concentration up to 17% of the total metallic sites, whereas at Al content larger than 31% the substitution is energetically more favored on alternated metallic layers (Mg undoped planes alternate with Mg−Al layers). The formation of this Al-rich phase leads at 50% doping to the formation of the double omega $Mg_{1/2}Al_{1/2}B_2$ ordered lattice. At 1000 K from 17 to 31% the two phases, the disordered $Mg_{1-x}Al_xB_2$ (x=0.17) and the ordered $Mg_{1/2+y}Al_{1/2-y}B_2$ (y=0.19) lattices coexist.

This phase separation is energetically driven by the balance of the enthalpy and entropy contributions to the Gibbs energy and occurs in parallel with the variation of the superconductor properties of the overall $Mg_{1-x}Al_xB_2$ ($0<x<0.5$) system. In Figure 3b the experimental superconductive T_c reported in the literature for the $Mg_{1-x}Al_xB_2$ system are shown.[8,10,15,16,32,33] The two gray areas in Figure 3b represent the predicted intervals of the two-phase region boundaries in the high temperatures range 1000−1300K. This temperature range is that typically used in the synthesis of the $Mg_{1-x}Al_xB_2$ samples.

The experimental superconductive T_c decreases going from pure MgB_2 to the double-ω $Mg_{0.5}Al_{0.5}B_2$ structure. However two different decreasing trends are clearly evident for aluminum concentration <17% and >31%. The $Mg_{1-x}Al_xB_2$ system for $x > 0.31$ shows a decreasing trend of the superconductive critical temperature larger than the corresponding trend in the composition range $0<x<0.17$. It is to be noted that our computational results predict the formation at large aluminum concentrations of a double-ω-like structure with doubled c-axis compared to the starting hP3 lattice. In this structure unaltered magnesium layers are alternated with partially substituted metallic planes containing both Al and Mg atoms.

On the contrary, at small aluminum concentrations, DFT-GGA calculations predict a random substitution, even on adjacent metallic planes, of Mg by aluminum atoms: this spacial organization is favored by the configurational entropy. The stability field of this disordered phase occurs in the range 0−17 atom % of Al substitution. Apparently in the same composition range the T_c decrease is smooth and does not show any drastic suppression of the superconductivity even at large Al doping.

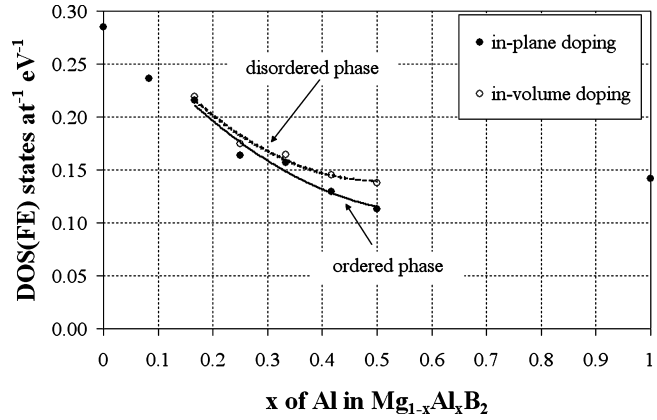

Figure 4. Variation of the density of the states at the Fermi energy with the aluminum content.

In the intermediate region 17−31 atom % of Al a large scattering of the T_c values is observed. In this composition range, our calculations predict the occurring of a phase separation: this two-phase stability field has also observed experimentally by many authors (see as e.g. refs 10, 14, and 15). On a qualitative basis we expect that this intermediate system, constituted by both the disordered and ordered phases, shows a more complicated and less easily predictable superconductive character. Indeed the specific morphology of the samples, the synthesis and annealing procedures, and the experimental methods could lead to large scattering in the measured low-temperature magnetization curves and therefore to the experimental T_c.

On the basis of all these experimental evidence we can conclude that present DFT-GGA calculations suggest that the suppression of the Al doping disorder in the metallic sublattice of MgB_2 driven by thermodynamics occurs in parallel with the collapse of the superconductive properties of the material.

Moreover it can be of interest to discuss this peculiar parallelism, i.e. the segregation of the ordered phase and the fading of the superconductor character of the $Mg_{1-x}Al_xB_2$ system, also in view of the accepted mechanism of the depression of the T_c due to the saturation of the σ bands of the MgB_2 by an increased number of valence electrons. Indeed it is now well understood that the Al doping fills the empty σ bands right above the Fermi level in the undoped MgB_2 thus leading to a decrease of the density of states (DOS) at the Fermi energy (E_F)[9,13,32] and to a topological change in the shape of the Fermi surfaces. Our calculations predict that the DOS at the Fermi energy for the in-plane and in-volume doped structures shows different decreasing trends: the pertinent variation with the aluminum content is shown in Figure 4. Indeed the density of states at E_F decreases from 0.28 states $eV^{-1}at^{-1}$ for the undoped oP36(0) lattice to 0.24 states $eV^{-1}at^{-1}$ for the oP36(1) structure. On further increasing the aluminum substitution, the DOS values at E_F progressively split for the in-volume and in-plane doped structures. Indeed in the so-called "disordered" structure, a larger DOS at the Fermi level is found, whereas in the "ordered" lattice a smaller one is calculated. This difference

increases monotonically from the 1% to the 22% for the oP36(2 L) and the oP36(6 L) lattices, respectively. Considering the different stability fields of the two disordered and ordered phases, it is likely to put into correlation the aforementioned variation of the DOS values at E_F with the decreasing trends of the T_c in the two composition ranges 0−17% and 31−50% of aluminum substitution.

Another effect that usually plays a role in the suppression of the T_c in multiband superconducting materials is the increase of the scattering due to nonmagnetic impurities. It has been reported[9] that in the case of the MgB_2 system the role of nonmagnetic impurities on the scattering is very weak,[34] particularly for Al. The only potential effect that could provide interband scattering is related to the buckling of the boron-layers and the subsequent out of plane disorder. Our calculation suggests that the buckling in both the cases of the in-plane or in-volume doping is similar and limited to a corrugation of the boron honeycomb smaller than <0.1 Å. On passing one can speculate that, by combining this result with the aforementioned trends of the DOS at E_F, the experimental spread in T_c values observed in the mixed phase region of the phase diagram (Figure 3) could be correlated to the splitting in the DOS values, rather than due to different impurity scattering.

However any further quantitative analysis or conclusion about the effect of the out of plane disorder here sketched is beyond the capabilities of the computational approach adopted and would require the calculation of the phonon spectra and of the electron−phonon coupling constants.

Acknowledgment. This research has been carried out using the CASPUR consortium computational resources under a "BANDO B 2007" grant entitled "Electronic and dynamic properties of MgB_2 and related composition modulated superstructures".

References

(1) Service, R. F. *Science* **2001**, *291*, 1476.

(2) Kortus, J. *Phys. C (Amsterdam, Neth.)* **2007**, *456*, 54.

(3) Balducci, G.; Brutti, S.; Ciccioli, A.; Gigli, G.; Manfrinetti, P.; Palenzona, A.; Butman, M.; Kudin, L. *J. Phys. Chem. Solids* **2005**, *66*, 292.

(4) Tomsic, M.; Rindfleisch, M.; Yue, J.; McFadden, K.; Phillips, J.; Sumption, M. D.; Bhatia, M.; Bohnenstiehl, S.; Collings, E. W. *Int. J. Appl. Ceram. Technol.* **2007**, *4*, 250.

(5) Canfield, P. C.; Crabtree, G. W. *Phys. Today* **2003**, *56*, 34.

(6) Ummarino, G. A.; Gonnelli, R. S.; Bianconi, A. *J. Supercond.* **2005**, *18*, 791.

(7) Slusky, J. S.; Rogado, N.; Regan, K. A.; Hayward, M. A.; Kalifah, P.; Inumaru, T. He.; Loureiro, S. M.; Haas, M. K.; Zandbergen, H. W.; Cava, R. J. *Nature* **2001**, *410*, 343.

(8) Agrestini, S.; Metallo, C.; Filippi, M.; Campi, G.; Manipoli, C.; De Negri, S.; Giovannini, M.; Saccone, A.; Latini, A.; Bianconi, A. *J. Phys. Chem. Solids* **2004**, *65*, 1479.

(9) Kortus, J.; Dolgov, O. V.; Kremer, R. K.; Golubov, A. A. *Phys. Rev. Lett.* **2005**, *94*, 027002.

(10) Kasinathan, D.; Lee, K. W.; Pickett, W. E. *Phys. C (Amsterdam, Neth.)* **2005**, *424*, 116.

(11) Profeta, G.; Continenza, A.; Bernardini, F.; Satta, G.; Massidda, S. *Int. J. Mod. Phys. B* **2002**, *16*, 1563.

(12) Bernardini, F.; Massidda, S. *Europhys. Lett.* **2006**, *76*, 491.

(13) Cava, R. J.; Zandberegen, H. W.; Inumaru, K. *Phys. C (Amsterdam, Neth.)* **2003**, *385*, 8.

(14) Palmisano, V.; Simonelli, L.; Puri, A.; Fratini, M.; Busby, Y.; Parasiades, P.; Liarokapis, E.; Brunelli, M.; Fitch, A. N.; Bianconi, A. *J. Phys.: Condens. Matter* **2008**, *20*, 434222.

(15) Mugdel, M.; Awana, V. P. S.; Kishan, H.; Bhalla, G. L. *Phys. C (Amsterdam, Neth.)* **2007**, *467*, 31.

(16) Karpinski, J.; Zhigadlo, N. D.; Schuck, G.; Kazakov, S. M.; Batlogg, B.; Rogacki, K.; Puzniak, R.; Jun, J.; Muller, E.; Wagli, P.; Gonnelli, R.; Daghero, D.; Ummarino, G. A.; Stepanov, V. A. *Phys. Rev. B* **2005**, *71*, 174506.

(17) Margadonna, S.; Prassides, K.; Arvanitidis, I.; Pissas, M.; Papavassiliou, G.; Fitch, A. N. *Phys. Rev. B* **2002**, *66*, 014518.

(18) Barabash, S. V.; Stroud, D. *Phys. Rev. B* **2002**, *66*, 012509.

(19) Profeta, G.; Continenza, A.; Bernardini, F.; Monni, M.; Massidda, S. *Supercond. Sci. Technol.* **2003**, *16*, 137.

(20) Profeta, G.; Continenza, A.; Massidda, S. *Phys. Rev. B* **2003**, *68*, 144508.

(21) Singh, P. P. *Bull. Mater. Sci.* **2003**, *26*, 131.

(22) Liu, J.; Zhao, Y.; Yi, L. *Comm. Theo. Phys. (Beijing)* **2008**, *49*, 504.

(23) de la Pena, O.; Aguayo, A.; de Coss, R. *Phys. Rev. B* **2002**, *66*, 012511.

(24) Perdew, J. P.; Wang, Y. *Phys. Rev. B* **1992**, *45*, 13244.

(25) Baroni, S.; Dal Corso, A.; de Gironcoli, S.; Giannozzi, P.; Cavazzoni, C.; Ballabio, G.; Scandolo, S.; Chiarotti, G.; Focher, P.; Pasquarello, A.; Laasonen, K.; Trave, A.; Car, R.; Marzari, N.; Kokalj, A. http://www.pwscf.org accessed 13/05/2009.

(26) Monkhorst, H. J.; Pack, J. D. *Phys. Rev. B* **1976**, *13*, 5188.

(27) MacDonald, A. H.; Vosko, S. H.; Coleridge, P. T. *J. Phys. C Solid State Phys.* **1979**, *12*, 2991.

(28) Villars, P. *Pearson's Handbook of Crystallographic Data*; ASM International: Materials Park, OH, 1997 (lattice structures given in alphabetical order of the corresponding chemical formula).

(29) van Setten, M. J.; Uijttewaal, M. A.; de Wijs, G. A.; de Groot, R. A. *J. Am. Chem. Soc.* **2007**, *129*, 2458.

(30) Gurvich, L. V.; Iorish, V. S. *IVTANTHERMO-Database of thermodynamic properties of individual substances*. Thermocentre of the Russian Academy of Science. Begell House: New York, 1993 (Software Vers. 1.01).

(31) Domalski, E. S.; Armstrong, G. T. *J. Res. Nat. Bureau Stand. A* **1967**, *71*, 307.

(32) Bianconi, A.; Agrestini, S.; Di Castro, D.; Campi, G.; Zangari, G.; Saini, N. L.; Saccone, A.; De Negri, S.; Giovannini, M.; Profeta, G.; Continenza, A.; Satta, G.; Massidda, S.; Cassetta, A.; Pifferi, A.; Colapietro, M. *Phys. Rev. B* **2002**, *65*, 174515.

(33) Putti, M.; Affronte, M.; Manfrinetti, P.; Palenzona, A. *Phys. Rev. B* **2003**, *68*, 094514.

(34) Mazin, I. I.; Andersen, O. K.; Jepsen, O.; Dolgov, O. V.; Kortus, J.; Golubov, A. A.; Kuzmenko, A. B.; van der Marel, D. *Phys. Rev. Lett.* **2002**, *89*, 107002.

CT900167K